
Volume 309 Issue 2 1 December 2007 ISSN 0022-0248

JOURNAL OF CRYSTAL GROWTH

Available online at www.sciencedirect.com
ScienceDirect
Journal of Crystal Growth 309 (2007) 197–215
JOURNAL OF CRYSTAL GROWTH
www.elsevier.com/locate/jcrysgro

Growth of equiaxed dendritic crystals settling in an undercooled melt, Part 1: Tip kinetics

A. Badillo, D. Ceynar, C. Beckermann*

Department of Mechanical and Industrial Engineering, The University of Iowa, 2402 Seamans Center, Iowa City, IA 52242, USA

Communicated by G.B. McFadden
Available online 21 September 2007

Abstract

Experiments are conducted to measure the dendrite tip growth velocities of equiaxed crystals of the transparent model alloy succinonitrile–acetone that are settling in an undercooled melt. The tip velocities are measured as a function of the crystal settling speed and the Eulerian angle between the dendrite arms and the flow direction relative to the crystal. The ratio of the settling speed (or flow velocity) to the tip growth velocity ranges from 62 to 572. The ratio of the measured tip velocity to that predicted from a standard diffusion theory for free dendritic growth ranges from almost zero for dendrite tips growing in the wake of the crystal, about unity for dendrite tips with an orientation close to normal to the flow direction, and up to two for dendrite tips growing into the flow. Despite the relatively strong flow relative to the crystal, the average tip growth velocity of the six primary dendrite arms of an equiaxed crystal is found to be in excellent agreement with the standard diffusion theory result. The individual tip velocities are correlated using a boundary layer model of free dendritic growth in the presence of melt flow that is modified to account for the flow angle dependence. Using the same dendrite tip selection parameter, σ^*, as established previously under purely diffusive conditions (0.02), good agreement is achieved between the measured and predicted tip velocities. The model is also found to predict well the variations in the tip velocity that occur during settling due to crystal rotation and settling speed changes.

PACS: 68.70.+w; 81.30.Fb

Keywords: A1. Convection; A1. Dendrites; A1. Growth models; B1. Succinonitrile

1. Introduction

Equiaxed dendritic crystals are frequently observed in metal alloy castings. They grow freely from small nuclei or solid fragments that are suspended in thermally and/or constitutionally undercooled melts. The term 'equiaxed' stems from the fact that for a cubic crystal structure, a seed develops six primary dendrite arms that grow at right angles to each other at approximately the same rate. Higher order dendrite arms are usually found behind the primary dendrite tips. During growth, solute and the latent heat of fusion are rejected into the undercooled liquid surrounding the crystal. Understanding the growth of such equiaxed dendritic crystals is crucial for modeling the evolution of the grain structure and the development of defects in castings [1–3]. In this respect, it is not sufficient to only model the growth kinetics of an isolated dendrite tip. The evolution of the dendritic solid structure behind the tip, internal to the crystal envelope, must also be considered. The growth of equiaxed crystals in castings usually takes place in the presence of considerable melt flow and buoyant movement (i.e., settling or floatation) of the crystals themselves. Such flow can influence the growth of an equiaxed crystal and, in turn, its movement relative to the melt. The objective of the present experimental study is to perform detailed measurements of the growth of equiaxed dendritic crystals that are settling in an undercooled melt. Both, the growth of the dendrite tips (Part 1) and the solid internal to the crystal envelope (Part 2), are examined. The experiments are intended to provide crucial input to, and validation of previously developed models of

*Corresponding author. Tel.: +1 319 335 5681; fax: +1 319 335 5669.
E-mail address: becker@engineering.uiowa.edu (C. Beckermann).

0022-0248/$ - see front matter © 2007 Elsevier B.V. All rights reserved.
doi:10.1016/j.jcrysgro.2007.09.018

equiaxed dendritic solidification in the presence of convection and crystal movement [4].

Previous experimental studies involving equiaxed dendritic crystals have primarily focused on the free growth of single, isolated dendrite tips into an undercooled melt. In particular, the microgravity experiments of Glicksman and coworkers [5], employing the transparent model substance succinonitrile (SCN), have resulted in a rather complete understanding of diffusion controlled dendrite tip growth. Corresponding experiments on earth [5–7] are generally influenced by natural convection in the melt. Additionally, some SCN experiments have been conducted where the melt is forced to flow past a stationary dendrite tip (e.g., Ref. [8]). For melt flow in a direction opposite to the dendrite tip growth direction, various convection models have been developed to predict the increase in the growth Péclet number due to melt flow, beyond the Ivantsov diffusion limit [9–11]. Comparisons between microgravity and terrestrial data have revealed that the dendrite tip selection parameter or stability constant σ^* for SCN does not change from the microgravity value of about 0.02 due to the presence of natural convection in the melt [5,11–13]. For larger flow velocities, as may be achieved in forced convection experiments, Lee et al. [8] observed an increase in σ^* of up to 66%.

Dendrite tip growth during the settling of equiaxed crystals has been investigated by Ramani and Beckermann [14] and Appolaire et al. [15,16] using transparent ammonium chloride–water (NH_4Cl–H_2O) solutions. In those experiments, a single NH_4Cl crystal was dropped inside a tall cylindrical glass tube containing an otherwise quiescent undercooled solution. All three of these studies showed that dendritic growth is strongly affected by the flow relative to the settling crystal: the measured tip velocities, averaged over all six primary dendrite arms, were found to be between 15 and 68 times larger than those calculated from a theory that assumes purely diffusive solute transport in the melt. Comparisons with theories are hampered by the fact that the dendrite tip selection parameter σ^* and some of the properties are not well established for NH_4Cl dendrites. Liu et al. [17] measured a value of $\sigma^* = 0.026$ in their diffusion-controlled experiments. Appolaire et al. [15], on the other hand, estimated a value of $\sigma^* = 0.081$ based on a fit of measured tip growth velocities to theoretical predictions that account for melt flow. They attributed this 212% increase in σ^* to the fact that in their experiments the settling speeds of the crystals were from 330 to 1550 times larger than the tip growth velocities. The melt flow to dendrite tip growth velocity ratio in the previous forced convection experiments by Lee et al. [8], who observed an increase in σ^* of up to 66% for SCN, only extended to 255.

Another issue in the above-mentioned comparisons is that during the settling of equiaxed crystals, the flow relative to the dendrite tips is much more complex than that assumed in the theories. Only a dendrite tip that is pointing exactly downward during settling experiences a flow in a direction parallel, but opposite, to the growth direction (defined here as a flow angle, θ, of 0°). Some of the primary dendrite tips grow in a direction that is more perpendicular to the flow direction ($\theta \approx 90°$), while yet others are growing downstream of other dendrite arms or the entire crystal (θ approaching 180°). Furthermore, an equiaxed crystal often rotates during settling. Hence, the angles between the six primary tip growth axes and the flow direction can change continuously. Previous studies have shown that the tip growth velocity depends strongly on the flow angle [9,18]. Certainly, the average growth velocity of the six primary dendrite arms cannot be expected to be equal to the tip growth velocity for a zero flow angle. Another complication is that the melt in the wake region of a settling equiaxed crystal is less undercooled than the melt of the original composition and temperature. Here, the term wake refers to the downstream region where solute and heat rejected by upstream dendrite arms modifies the local melt undercooling. A clear illustration of this effect is provided by the phase-field simulations of dendritic growth with forced melt flow by Tong et al. [19] and others. They showed that the downstream dendrite tip growth velocity in the wake of an equiaxed crystal is generally smaller than the one corresponding to purely diffusive transport for the original melt undercooling.

The above review indicates that there is much to be learned about the growth of equiaxed dendritic crystals in the presence of relative movement between the crystal and the melt. The present settling experiments are conducted in a setup similar to that employed by Ramani and Beckermann [14], but the transparent model alloy used is SCN–acetone. This alloy is well suited for such experiments because measurements of dendritic growth of pure SCN and SCN–acetone alloys have been performed under a variety of conditions in the past, and because all relevant thermophysical properties are known accurately [5–7]. In particular, Ceynar and Beckermann [20] performed careful measurements of the density of SCN–acetone alloys. Since the density difference between solid and liquid SCN is about 3%, the crystal settling speeds would be similar to those in metallic alloys. In this paper (Part 1), measurements of the growth velocities of each of the six primary dendrite arms of an equiaxed crystal are presented and analyzed as a function of the settling speed and the orientation of the arms with respect to the flow. The measurements are compared to available theories of dendritic growth.

2. Experimental setup and procedures

The present experiments on the growth of equiaxed dendritic crystals settling in an undercooled melt were performed using dilute SCN–acetone alloys of varying composition. The alloys were prepared from 99.97% pure SCN, obtained by vacuum reflux distillation, and reagent grade acetone. A schematic of the experimental setup is shown in Fig. 1. The SCN–acetone alloy was filled into a

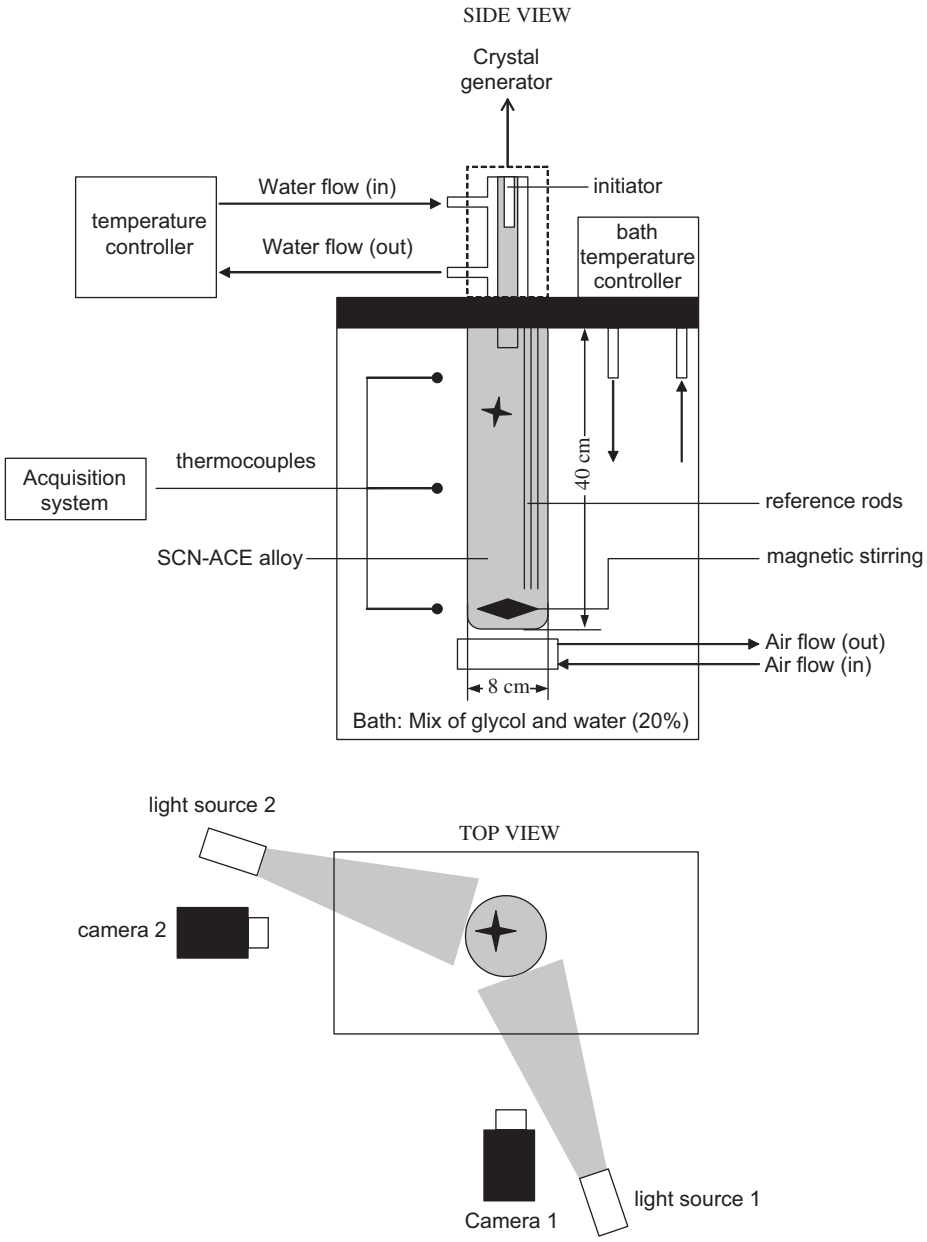

Fig. 1. Schematic illustration of the experimental setup.

40-cm-tall cylindrical glass column having an inner diameter of approximately 8 cm. The glass column was inserted into a large rectangular bath with transparent walls through which a temperature controlled ~20% glycol–water mixture was circulated. A glycol–water mixture was chosen to eliminate optical distortion by matching the refractive index of liquid SCN near its melting point to the bath liquid. The bath effectively maintained the SCN–acetone alloy at a constant and uniform temperature throughout the duration of an experiment. Using carefully calibrated thermocouples, the temperature of the SCN–acetone alloy within the glass column was verified to be within about 0.05 °C of the desired set point. A magnetic stirrer inside the glass tube served to homogenize the melt before an experiment. The entire system was sealed in order to avoid evaporation of the acetone and absorption of water vapor from the ambient air.

Small seeds, from which the equiaxed crystals were grown, were produced in-situ using a so-called 'crystal generator' located at the top of the 40-cm-long glass column. It consisted of a small glass tube protruding slightly past the free surface into the SCN–acetone alloy. The temperature of the crystal generator was controlled by a separate circulating bath. Melt was pulled from the test column into the crystal generator tube by the application of a slight vacuum. SCN crystals were nucleated on an internal glass rod ('initiator') by inserting a cooled copper rod into the initiator well. Under the action of gravity, some of the crystals separated from the glass rod and

settled through the generator tube. A small restriction near the end of the tube allowed for only one crystal to enter the column inside the tank; all other crystals were effectively blocked.

During the experiments, the location, size, shape, and orientation of the equiaxed crystals were measured as a function of time using two cameras. The cameras were placed on a manually operated, vertically moving platform at a right angle to each other, equidistant from the column, such that two orthogonal views of the equiaxed crystal were obtained at all times. Using a manual screw, the platform was moved vertically in order to track the crystal as it settled in the 40-cm-tall glass tube. Illumination of the crystal was obtained from two light sources placed next to the cameras and diffuse backlighting. Several small-diameter rods, with markings along their length, were placed inside the glass tube in order to provide a scale for the length measurements and a reference for determining the vertical position of the crystals. In order to calibrate the measurements, glass spheres of known diameter (between 1 and 5 mm) were submerged in the SCN–acetone melt. It was found that the length and position measurements from the images acquired by the two cameras were accurate to within ± 0.1 mm.

Before each experiment, the liquidus temperature of the SCN–acetone melt was measured. For this purpose, the temperature of the bath was set to a value where only a small amount of solid remained in the glass column. Then, the temperature was increased in small steps until the last solid just melted. At each step, the system was stirred and allowed to reach equilibrium by holding it at the given temperature for several hours. This way, it was possible to measure the liquidus temperature to an accuracy of ± 0.07 K. Knowing the slope of the SCN–acetone liquidus line (-2.8 K/wt%), the corresponding uncertainty in the solute concentration is ± 0.03 wt% acetone. After determining the liquidus temperature, the crystal generator was filled and the temperature of the bath was lowered, without nucleating any solid, until the desired melt undercooling was obtained. After reaching equilibrium, an experiment was started by activating the crystal generator.

Fig. 2 shows a typical image of a settling equiaxed dendrite. A similar image is obtained from the other camera. These two orthogonal images were then used to measure the instantaneous dimensions and orientation of the crystal, as well as its settling speed, U. Between four and five primary dendrite tips are visible on each image, implying that at least two dendrite tips are common to both images. Each of the six primary dendrite arms is visible in at least one image. First, straight lines were drawn on each image from the primary dendrite tips along the main trunks towards the center of the crystal. The point where the straight lines intersect was taken as the center of the crystal. It was observed that the primary dendrite arms grow, to within a few degrees, at right angles to each other (e.g., see Fig. 2). Thus, a unique intersection point of all straight lines could be identified to within about ± 0.1 mm.

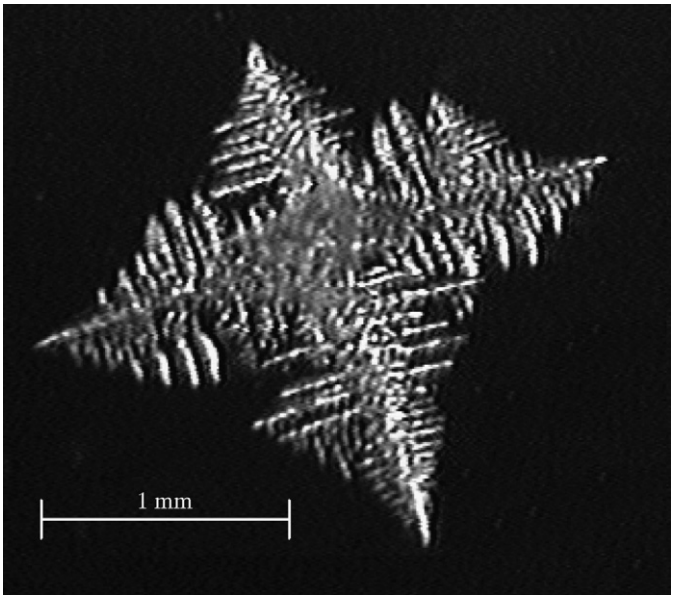

Fig. 2. Typical image of an equiaxed dendrite settling in the undercooled melt.

Knowing the coordinates of the primary tips and the center of the crystal on the two orthogonal images, and assuming that the primary dendrite arms grow at right angles to each other, it was relatively straightforward to calculate the tip position, the length (measured from the center of the crystal to the tip), L, and the orientation of each of the primary dendrite arms in three-dimensional space. Hence, the reported lengths were not just taken from the projections of the arms on the images, but represent actual dendrite arm lengths. From knowledge of the dendrite orientation in three-dimensional space, a Eulerian or polar angle, θ, between each of the six primary arms and a downward pointing vector (in the direction of gravity) was also determined. An arm pointing exactly downward has a Eulerian angle of 0°, and an arm pointing exactly upward has $\theta = 180^\circ$. Since the crystals settled in the downward direction, the Eulerian angle measured here is equivalent to the so-called flow angle defined in Section 1. The rotational angle of the dendrite arms, in the plane perpendicular to gravity, was not considered in the present analysis of the experimental data. The total uncertainty in the dendrite arm length measurements was estimated to be less than ± 0.2 mm. The uncertainty in the Eulerian or flow angle was approximately $\pm 5^\circ$.

3. Experimental results

The results of eight settling experiments are presented here, as summarized in Table 1. The acetone concentration, C_0, ranged from about 1–4 wt% and the melt undercooling, ΔT, from 0.5 to 1.3 K. Smaller undercoolings did not provide for sufficient dendrite growth to allow for accurate measurements to be made, while larger undercoolings resulted in spurious nucleation of solid. Table 1 also

Table 1
Experimental conditions and summary of measurements

Experiment	C_0 (wt%)	ΔT (K)	$\bar{L}^i$ (mm)	$\bar{L}^f$ (mm)	$\bar{v}_t$ (μm/s)	U^i (mm/s)	U^f (mm/s)
1	1.08	0.53	1.99	3.21	15.2	3.47	5.93
2	1.08	0.54	2.14	3.41	15.9	4.05	7.38
3	1.08	0.84	2.00	5.69	46.1	3.01	8.11
4	1.40	0.47	1.26	1.85	7.4	2.64	4.23
5	2.96	0.82	1.56	2.48	11.5	2.62	4.20
6	2.96	1.3	1.57	4.26	33.6	2.08	5.57
7	3.97	0.75	1.03	1.51	6.0	1.91	1.94
8	3.97	1.23	1.94	3.65	21.4	1.74	4.33

summarizes the ranges of some of the measured quantities for each experiment. Between the various experiments, the settling speed, U, varied from about 1.7 mm/s (minimum initial value, U^i) to 8.1 mm/s (maximum final value, U^f), the average primary dendrite arm length, $\bar{L}$, from about 1 mm (minimum initial value, $\bar{L}^i$) to 5.7 mm (maximum final value, $\bar{L}^f$), and the average primary dendrite tip growth velocity, $\bar{v}_t$, from about 6–46 μm/s. The ratio of the settling speed to the average tip growth velocity, $U/\bar{v}_t$, ranged from 62 to 572.

3.1. Settling speed

The measured vertical locations of the crystal center (symbols) as a function of time are plotted for each of the eight experiments in Fig. 3. Typically, the settling was tracked for about 80 s. Crystal meandering in the lateral directions was observed to be negligibly small. A parabola (solid line) provided a near perfect fit of the measured data in each experiment. From this fit, the instantaneous settling speed, U, was calculated as the time rate of change of the crystal location in the downward direction, as shown by the dashed lines in Fig. 3. While the settling speed can be seen to increase in a linear fashion, the rate of increase is different for each experiment. The settling speed is determined by a balance between the crystal weight and its drag. A larger crystal will generally settle faster than a smaller one. However, the observed linear increase in the settling speed of a dendritic crystal during growth is not easily explained. The settling speed is a complex function of the mass and shape of the entire crystal. The measured settling speed variations are further analyzed in Part 2 of the present study.

3.2. Dendrite arm length and angle

The measured lengths (open circles) and Eulerian angles (solid squares) of the primary dendrite arms are plotted as a function of time in Figs. 4–11. These eight figures correspond to the eight experiments listed in Table 1, and the six plots in each figure contain the data for every one of the six primary dendrite arms. It can be seen that the six dendrite arms of a settling equiaxed crystal generally grow at different rates, even though the melt is uniformly undercooled. Furthermore, the arm length usually increases in a non-linear fashion, indicating a non-constant tip growth velocity. In experiments 1, 2, 7 and 8, the variations of the angles are relatively small, indicating that little crystal rotation took place during the settling process. On the other hand, strong crystal rotation can be inferred from the angle variations in experiments 3–6. Note that at any instant of time, the angles shown in the six plots of each figure add up to 540°, since the six primary dendrite arms grow at right angles to each other, and the average flow angle for all six arms is 90°. The crystal rotation can be explained by the different individual dendrite arm growth rates. For example, if during settling a downward growing arm with an Eulerian angle close to zero grows more quickly than the other arms, the drag force on that arm becomes larger than the drag force on the other arms and the crystal rotates until the longer arm points approximately upward.

The average length of the six primary dendrite arms of an equiaxed crystal, $\bar{L}$, is plotted in Fig. 12 as a function of time. As opposed to the individual arm length data, the calculated averages vary in an almost perfect linear fashion in all eight experiments. This indicates that the *average* tip growth velocity of a settling equiaxed dendrite, $\bar{v}_t$, is constant. The average tip growth rate is constant despite the settling speed continually increasing during an experiment. The slopes of the average dendrite arm length variations are different for each of the eight experiments in Fig. 12, which is not unexpected since the melt undercooling and solute concentration vary among the experiments. These experimental observations are further discussed in the next section.

3.3. Discrete dendrite tip growth velocities

The measured arm length variations were also used to determine discrete dendrite tip growth velocities as a function of the Eulerian (or flow) angle and the settling speed. Tip growth velocities were obtained from the slopes of relatively short, straight line segments that were fit to the arm length versus time data in Figs. 4–11. Thus, they represent the tip speed relative to the center of the dendrite.

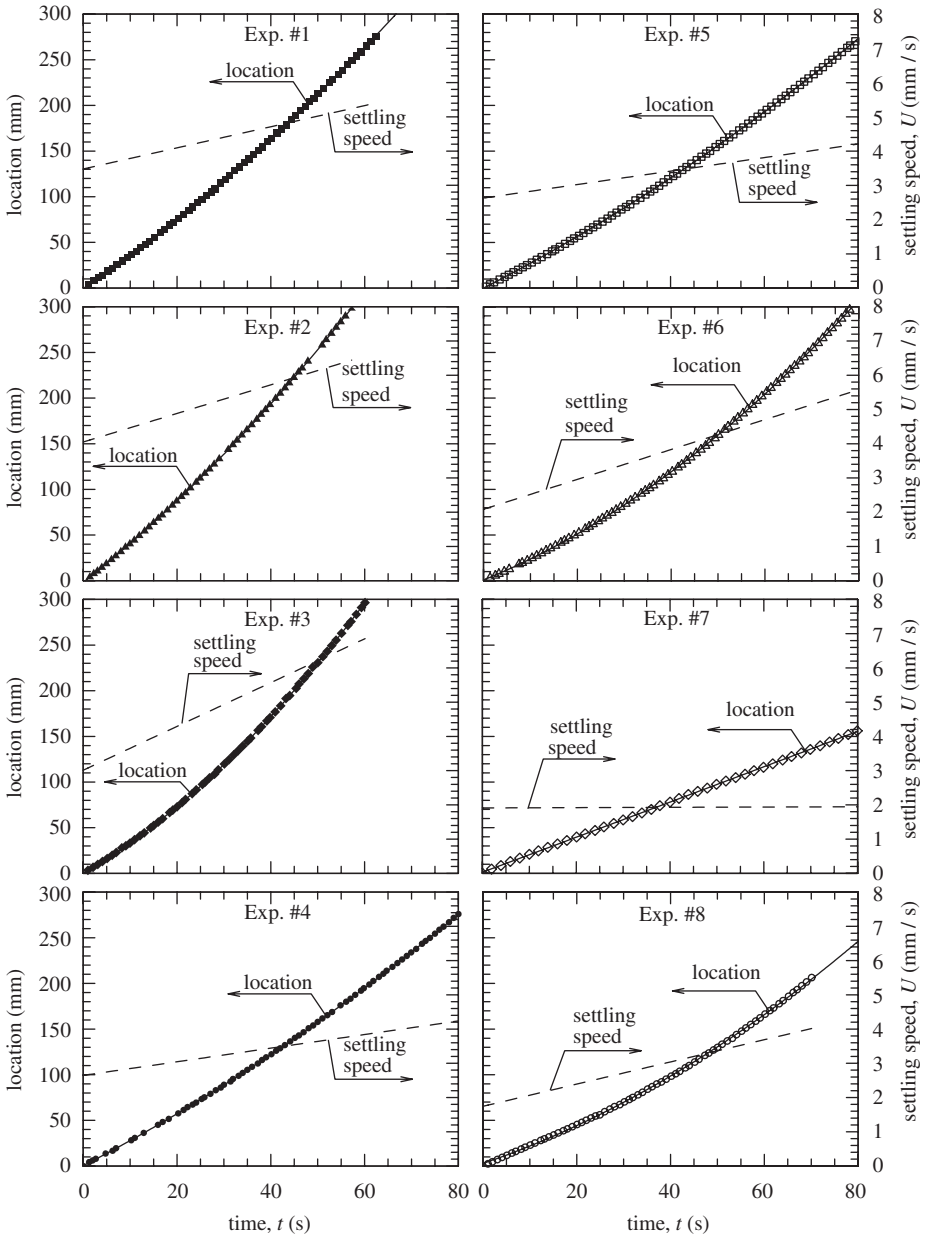

Fig. 3. Measured equiaxed dendrite locations as a function of time (symbols) and parabolic fit (solid lines), and corresponding settling speeds (straight dashed lines).

As already noted, the growth rate of a dendrite arm can vary considerably during an experiment. Therefore, the fits were limited to time periods between 10 and 40 s, and strong variations in the dendrite tip growth rate were avoided altogether. Furthermore, the fits were also limited to time periods over which the angle did not vary by more than about $\pm 15^{\circ}$. In other words, arm length data that correspond to very steep angle variations (e.g., 120° between 25 and 40 s for arm 1 in experiment 3; Fig. 6) were also excluded from the fits. The variations in the settling speed over the time periods of the fits were less than about ± 0.5 mm/s. Larger variations in the angle and settling speed during the fitting periods would not allow for a meaningful interpretation of the tip growth velocity data. Due to the above limitations, only one to three discrete tip growth velocities were obtained for each dendrite arm. The tip growth velocities obtained in this manner are listed in Table 2, together with the time periods of the fits and the average values of the Eulerian angle and settling speed. It should be mentioned that attempts were made to fit the arm length data to higher-order polynomials, instead of straight line segments, in order to obtain continuous variations of the dendrite tip growth velocity. This proved to be impractical due to occasional large scatter in the arm length data and the sometimes very abrupt changes in the growth velocity.

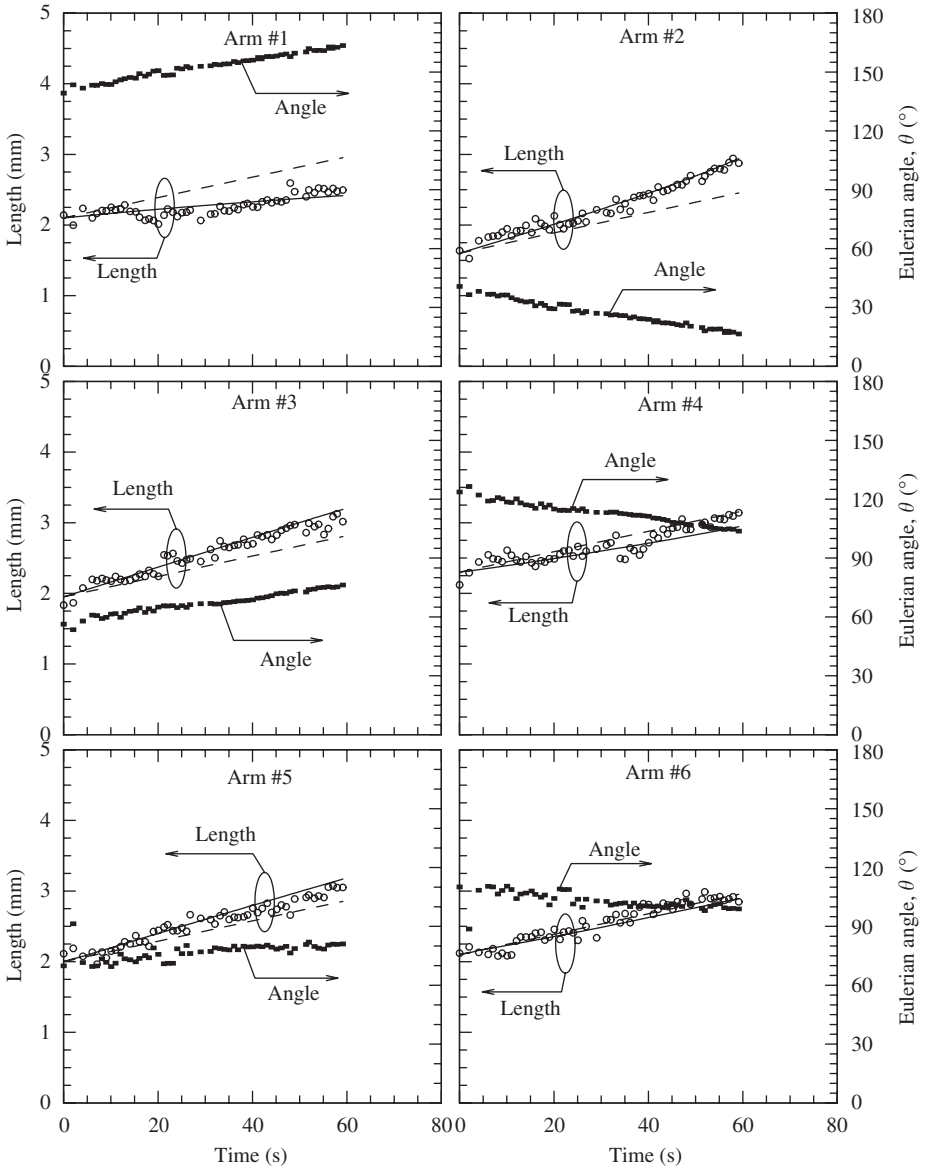

Fig. 4. Measured dendrite arm lengths (open circles) and Eulerian angles (solid squares) as a function of time for experiment 1, and predicted dendrite arm lengths from the diffusion theory (dashed line) and the convection model (solid line).

4. Comparison with theories and correlation of data

The measured data are first compared to the standard diffusion theory for free dendritic growth of an alloy into an undercooled melt [21–24]. This allows for a preliminary examination of the effect of the melt flow relative to the crystal. Then, a boundary layer model of convection is used to correlate the measured dendrite tip growth velocities as a function of the flow angle and the settling speed.

4.1. Comparison with diffusion theory

The standard theory of free dendritic growth for a binary alloy with diffusive heat and solute transport in the melt at low undercoolings [21–24] can be summarized as follows. Taking into account the capillary correction and neglecting the effects of interface attachment kinetics, the total imposed undercooling is composed of

$$\Delta T = \Delta T_{\mathrm{T}} + \Delta T_{\mathrm{C}} + \Delta T_{\mathrm{R}}, \tag{1}$$

where ΔT_{T}, ΔT_{C}, and ΔT_{R} are the thermal, solutal, and capillary contributions to the undercooling, respectively. The dimensionless thermal and solutal undercoolings are defined, respectively, as

$$\Omega_{\mathrm{T}} = \frac{T_{\mathrm{t}}^{*} - T_0}{L_{\mathrm{f}}/c_{\mathrm{l}}} \quad \text{and} \quad \Omega_{\mathrm{C}} = \frac{C_{\mathrm{t}}^{*} - C_0}{C_{\mathrm{t}}^{*}(1-k)}, \tag{2}$$

where L_{f} is the latent heat of fusion; c_{l} is the liquid specific heat; k is the partition coefficient; T_0 and C_0 are the initial or far-field melt temperature and solute concentration, respectively; and T_{t}^{*} and C_{t}^{*} are the temperature and solute concentration in the liquid at the dendrite tip, respectively.

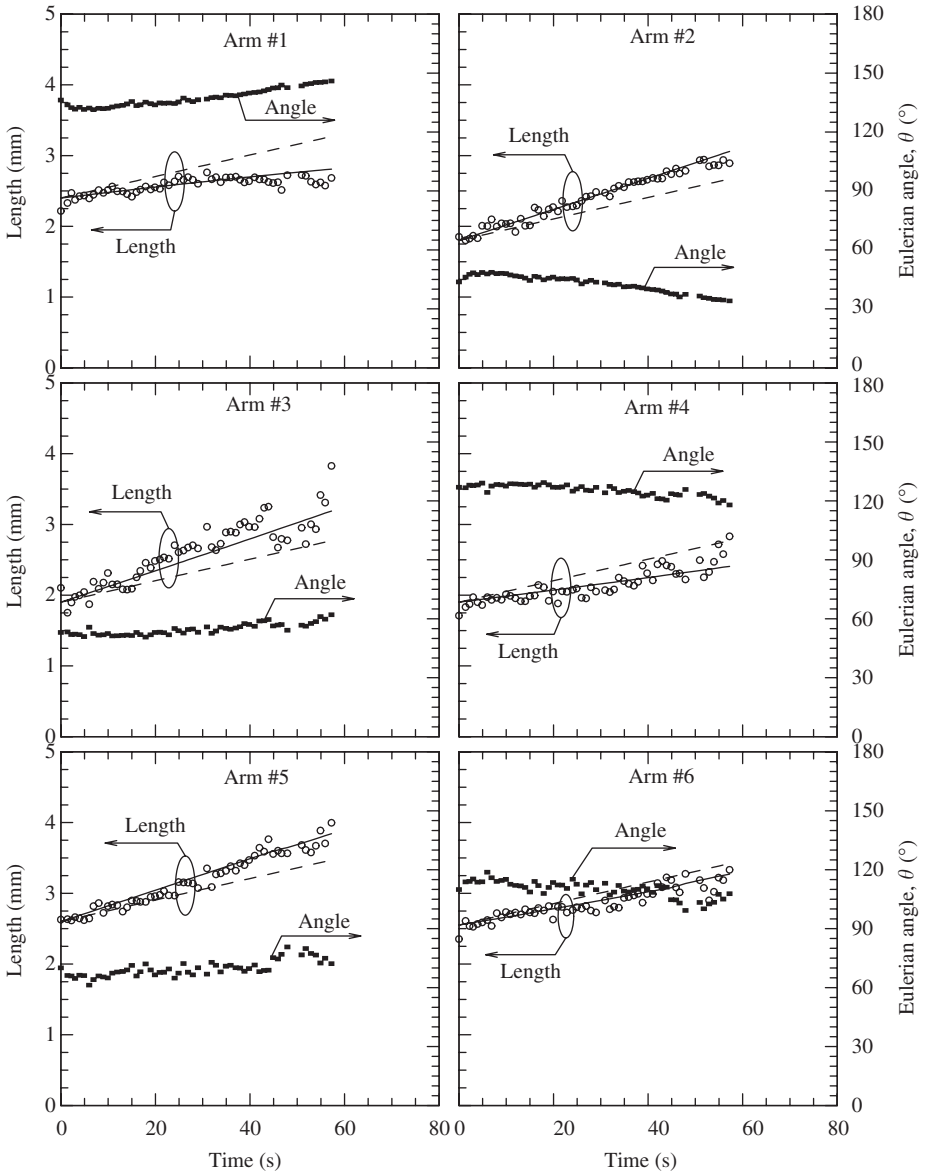

Fig. 5. Measured dendrite arm lengths (open circles) and Eulerian angles (solid squares) as a function of time for experiment 2, and predicted dendrite arm lengths from the diffusion theory (dashed line) and the convection model (solid line).

Approximating the capillary correction using the Gibbs–Thomson relation, Eq. (1) can be rewritten as

$$\Delta T = \frac{L_f}{c_l}\Omega_T + \frac{k\,\Delta T_0\,\Omega_C}{1-(1-k)\Omega_C} + \frac{2\Gamma}{R}, \tag{3}$$

where Γ is the Gibbs–Thomson coefficient; R is dendrite tip radius of curvature; and $\Delta T_0 = mC_0(1-(1/k))$ is the equilibrium freezing temperature range, in which m is the liquidus slope. The dimensionless thermal and solutal undercoolings in Eq. (3) are obtained from the Ivantsov solutions for quasi-steady heat and species diffusion around a paraboloid of revolution, which can be written in terms of the thermal ($Pe_T = v_t R/2\alpha_l$) and solutal ($Pe_C = v_t R/2D_l = LePe_T$) Péclet numbers as

$$\Omega_T = \mathrm{Iv}(Pe_T) \quad \text{and} \quad \Omega_C = \mathrm{Iv}(Pe_C), \tag{4}$$

where Iv is the Ivantsov function, D_l is the liquid mass diffusivity, α_l is the liquid thermal diffusivity, and $Le = \alpha_l/D_l$ is the Lewis number. Introducing the stability constant or selection parameter σ^*, the dendrite tip radius in the above equations is given by

$$R = \frac{d_0}{\sigma^*\left[\left\{2Pe_C((k\,\Delta T_0)/(L_f/c_l))/1-(1-k)\Omega_C\right\} + Pe_T\right]}, \tag{5}$$

where $d_0 = \Gamma/(L_f/c_l)$ is the capillary length. The selection parameter σ^* is constant with respect to the undercooling and C_0 variations [24].

The above set of equations was solved for the dendrite tip growth velocity, v_t, as a function of the total imposed melt undercooling, ΔT, and the alloy concentration, C_0,

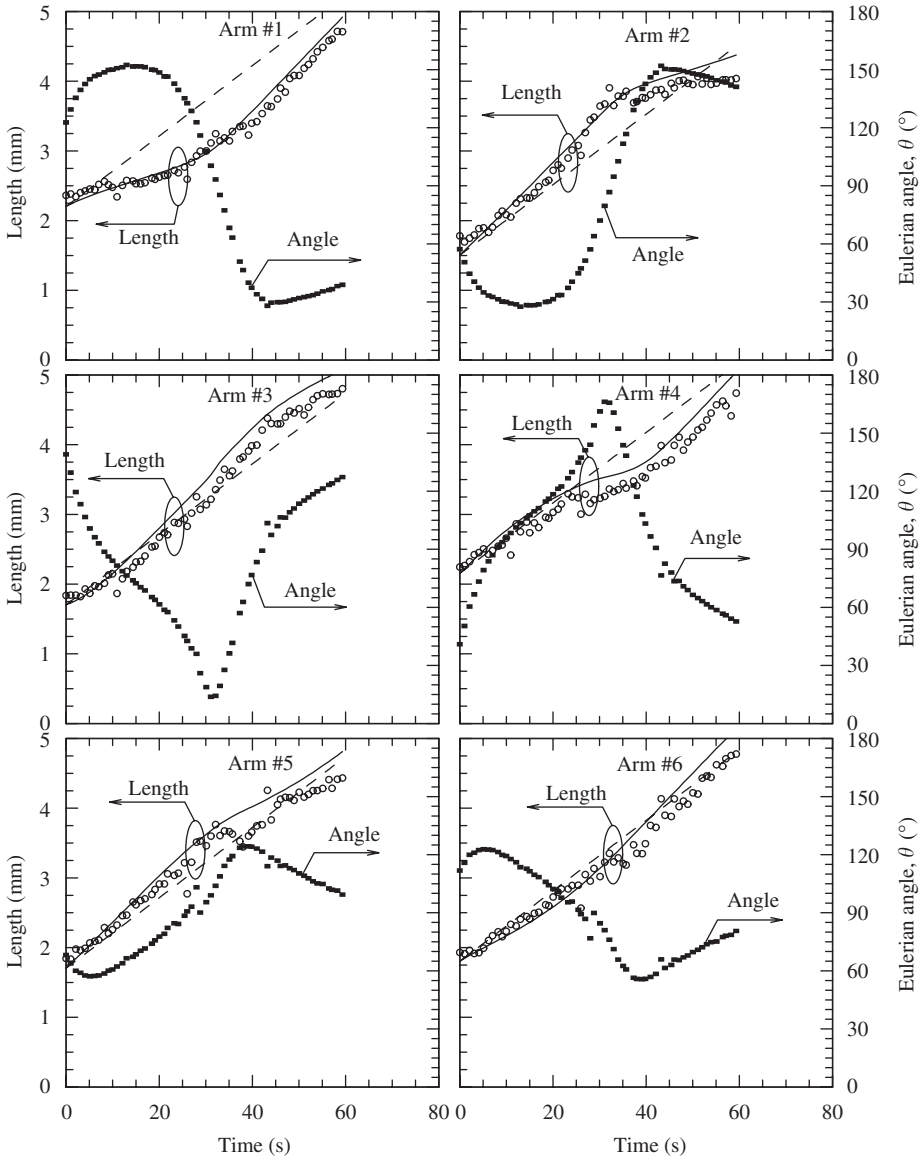

Fig. 6. Measured dendrite arm lengths (open circles) and Eulerian angles (solid squares) as a function of time for experiment 3, and predicted dendrite arm lengths from the diffusion theory (dashed line) and the convection model (solid line).

and for the SCN–acetone properties summarized in Table 3. The selection parameter σ^* was taken equal to the well-established diffusion value of 0.02. Since for purely diffusive transport the predicted tip velocity is constant, the length of a dendrite arm as a function of time can be calculated from

$$L = L^{\mathrm{i}} + v_{\mathrm{t}} t, \tag{6}$$

where t is the time from the beginning of the measurements and L^{i} is the measured initial length of a dendrite arm (at $t = 0$).

The predicted dendrite arm length variations are included in Figs. 4–11 as dashed lines. While the dashed lines in each of the six plots for an experiment have the same slope, they are shifted vertically since the six primary dendrite arms have different initial lengths, L^{i}. As expected, arm length variations from the diffusion theory generally do not agree with the measurements due to the effects of convection. Some measured arm lengths are above while others are below the predictions. In addition, the highly non-linear arm length variation observed in some of the experiments (e.g., Fig. 6), which indicates a non-constant tip growth velocity, is obviously not captured by the diffusion theory.

An interesting behavior is shown in Fig. 12. For all the eight experiments, the predictions from the diffusion theory (dashed lines) can be seen to be in almost perfect agreement with the measured average arm length variations (symbols). Slight differences occur in the latter parts of experiments 3 and 6, the origin of which is unknown. This good agreement with the diffusion theory is surprising, since it indicates that the relative flow between the crystal

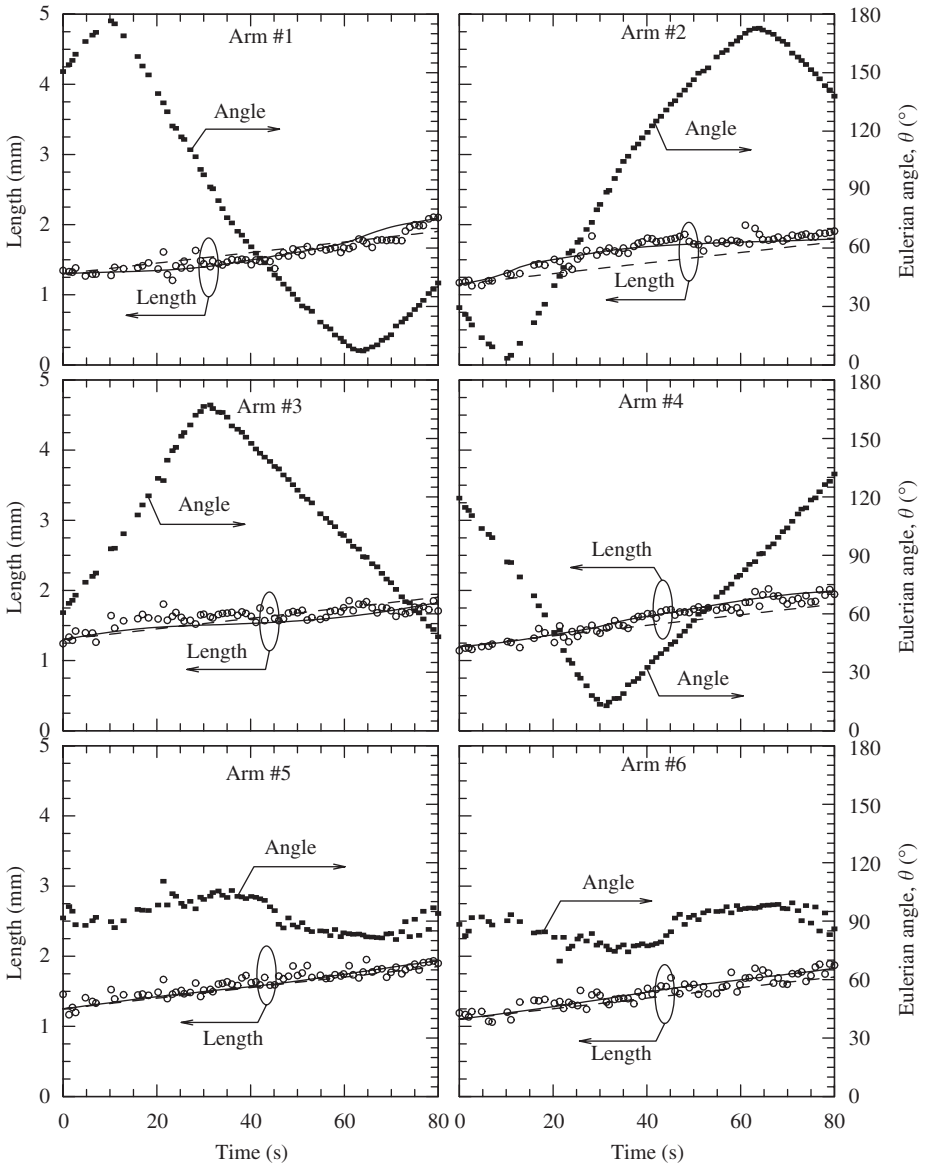

Fig. 7. Measured dendrite arm lengths (open circles) and Eulerian angles (solid squares) as a function of time for experiment 4, and predicted dendrite arm lengths from the diffusion theory (dashed line) and the convection model (solid line).

and the melt during settling has no effect on the average dendrite tip growth velocity in the present experiments. Ramani and Beckermann [14] and Appolaire et al. [15,16] found that the measured average growth velocities in their NH_4Cl–H_2O settling experiments were between 15 and 68 times larger than those predicted by a diffusion theory. The settling speed to average growth velocity ratio in the NH_4Cl–H_2O experiments ranged from 330 to 1550, while it ranged from 62 to 572 in the present SCN–acetone experiments. This difference is not significant enough to explain the much higher average tip growth velocities during settling in the NH_4Cl–H_2O experiments.

The effect of convection on the growth of settling SCN crystals is further illuminated in Fig. 13. Here, the measured dendrite tip growth velocities for each dendrite arm, as listed in Table 2, and normalized by the diffusive growth velocity predicted for each experiment, v_{meas}/v_{diff}, are shown as a function of the measured Eulerian angle in a polar plot. Generally, the tip growth velocities decrease with the Eulerian angle increasing from 0° to 180°. The dendrite arms with a Eulerian angle greater than about 90° have a growth velocity that is smaller than the diffusion value, i.e., the ratio v_{meas}/v_{diff} is less than unity. In fact, the smallest normalized dendrite tip growth velocities, for Eulerian angles close to 180°, approach zero. As already mentioned in Section 1, the arms in the wake of the equiaxed dendrite grow in a less undercooled melt, since heat and solute rejected by upstream arms is advected around the crystal. Hence, their tip velocities can be reduced to a value below the diffusion value corresponding to the original undercooling, despite the presence of convection. This finding is in contradiction to the

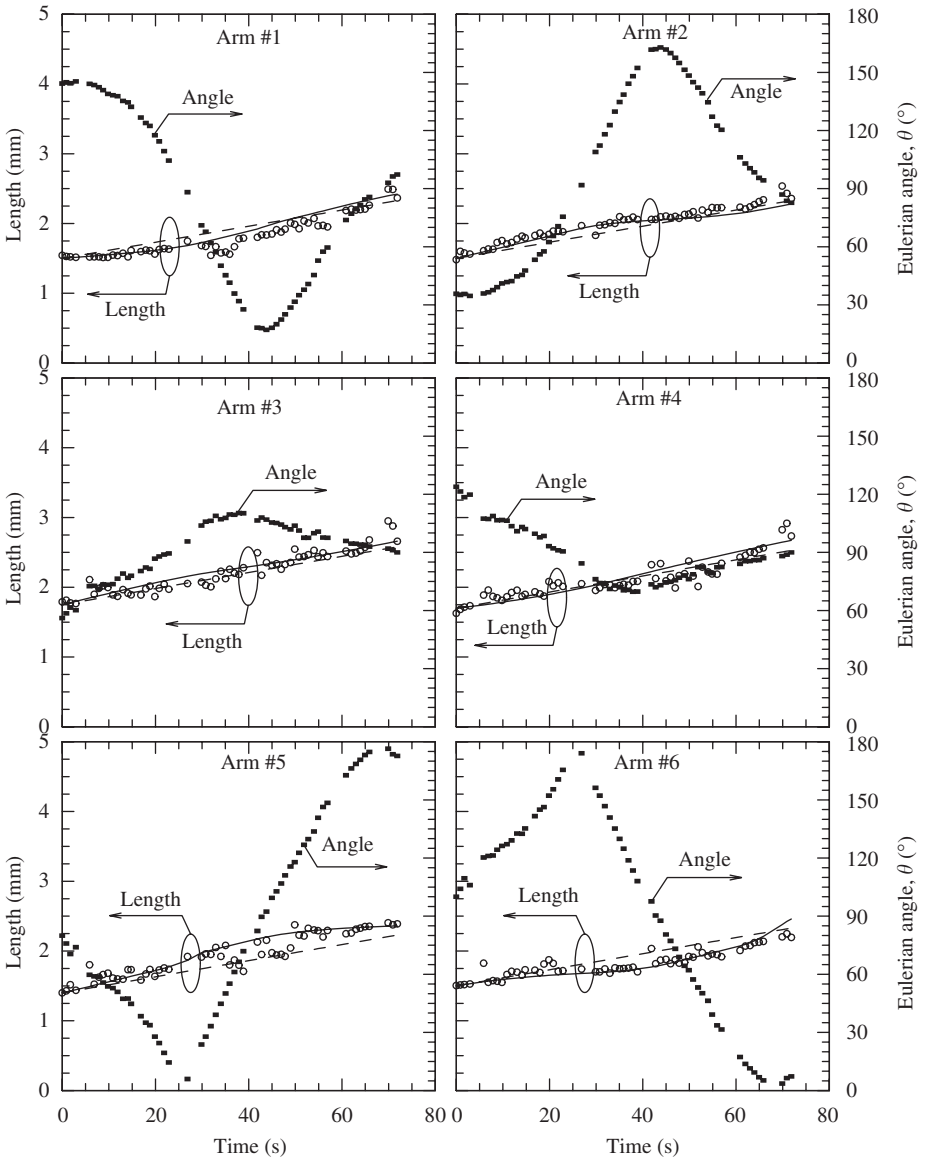

Fig. 8. Measured dendrite arm lengths (open circles) and Eulerian angles (solid squares) as a function of time for experiment 5, and predicted dendrite arm lengths from the diffusion theory (dashed line) and the convection model (solid line).

convection models by Sekerka et al. [9] and Gandin et al. [18], which give dendrite tip growth velocities as a function of the Eulerian angle that are always greater than the diffusion value.

It can also be seen in Fig. 13 that for Eulerian angles between 0° and 90° the growth velocity ratio, v_{meas}/v_{diff}, is generally greater than unity. This can be explained by the enhancement of the heat and solute transport at the dendrite tips by the flow, since for these angles the flow is more or less impinging on the dendrite tips and the melt undercooling is not reduced by upstream dendrite arm heat and solute rejection. For the present set of experiments, the maximum growth velocity ratio, v_{meas}/v_{diff}, observed is approximately equal to 2 for a flow angle of about 20°. However, at the same angle, ratios close to unity are found as well in Fig. 13. These variations should not be interpreted as experimental scatter. Clearly, the ratio v_{meas}/v_{diff} is not only a function of the Eulerian angle. For a given Eulerian angle, the growth velocity ratio still depends on the settling speed, and this dependency can change with melt undercooling and solute concentration. As can be seen from Table 2, the results in Fig. 13 cover a wide range of settling speeds and other growth conditions.

4.2. Correlation of tip growth velocity data using a boundary layer model of convection

Numerous theories have been developed to model the effects of convection on free dendritic growth, as reviewed by Li and Beckermann [11]. Boundary layer models have emerged as a relatively simple, but accurate means of representing the convection effect for flow opposite to the

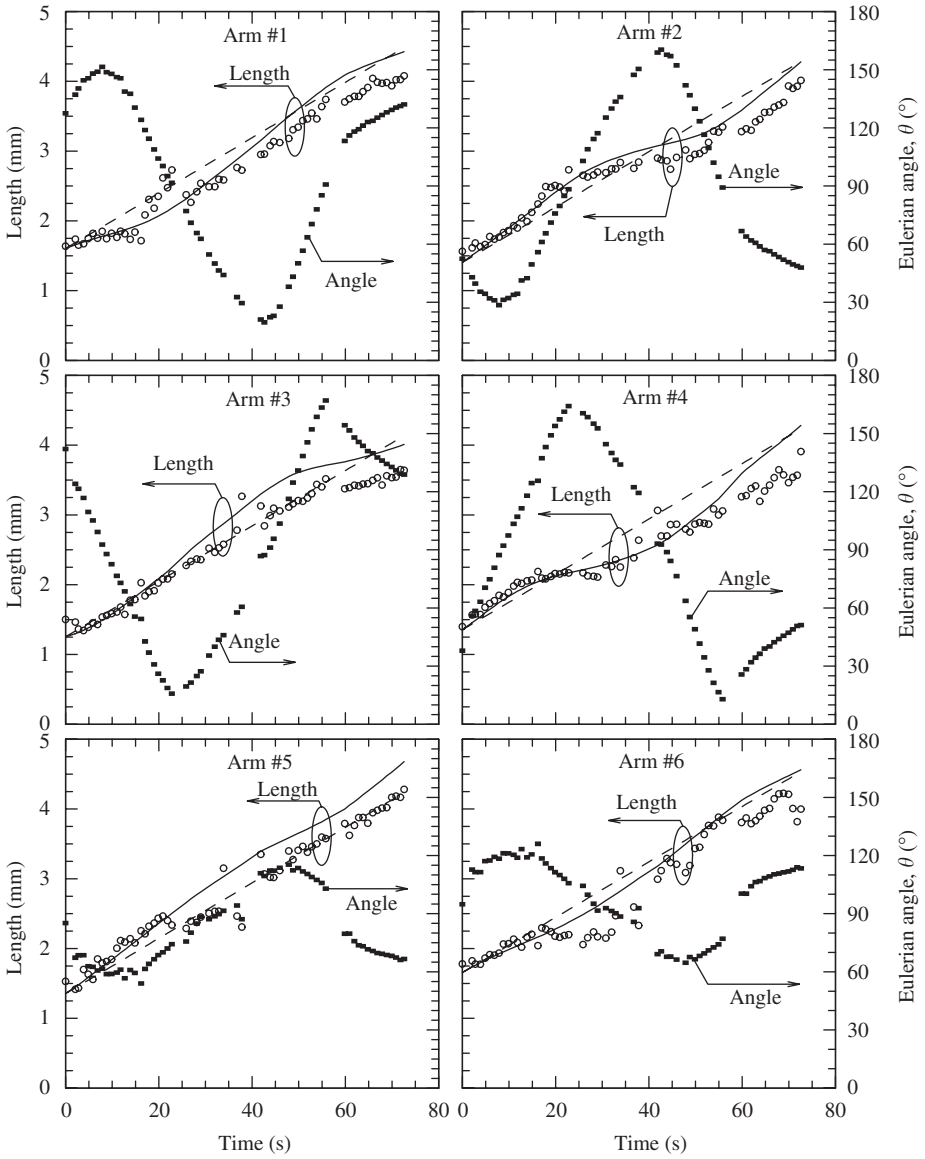

Fig. 9. Measured dendrite arm lengths (open circles) and Eulerian angles (solid squares) as a function of time for experiment 6, and predicted dendrite arm lengths from the diffusion theory (dashed line) and the convection model (solid line).

dendrite tip growth direction (i.e., $\theta = 0^\circ$) [9,11,18,25]. This approach is followed in the present study, but a modification is introduced to account for the flow angle dependency. The Ivantsov relations for the dimensionless thermal and solutal undercoolings as a function of the growth Péclet numbers, Eq. (4), are replaced by the following modified stagnant film solution of Cantor and Vogel [26]:

$$\Omega_T = Pe_T \exp(Pe_T)\left\{ E_1(Pe_T) - f(\theta)\, E_1\left[Pe_T\left(\frac{1+2\delta_T}{R}\right)\right]\right\} \tag{7}$$

and

$$\Omega_C = Pe_C \exp(Pe_C)\left\{ E_1(Pe_C) - f(\theta)\, E_1\left[Pe_C\left(\frac{1+2\delta_C}{R}\right)\right]\right\}, \tag{8}$$

where E_1 is the exponential integral function, and δ_T and δ_C are the thermal and solutal boundary layer thicknesses, respectively. The above two equations reduce to the Ivantsov relations given by Eq. (4) for infinitely large boundary layer thicknesses or for $f(\theta) = 0$, since $\mathrm{Iv}(Pe) = Pe \exp(Pe)E_1(Pe)$. The present modification relates to the addition of a so-called flow direction factor $f(\theta)$, which is equal to unity in the original stagnant film model. All other parts of the model, in particular the selection criterion given by Eq. (5), are identical to the diffusion theory presented in the previous section. The stability constant or selection parameter, σ^*, is taken equal to the diffusion value of 0.02, which can be justified by fact that the measured tip growth velocities are at most twice as large as the calculated diffusion values. Li and Beckermann [11] recently verified that $\sigma^* = 0.02$ works well for the terrestrial SCN and SCN–acetone dendrite growth data in Koss et al.

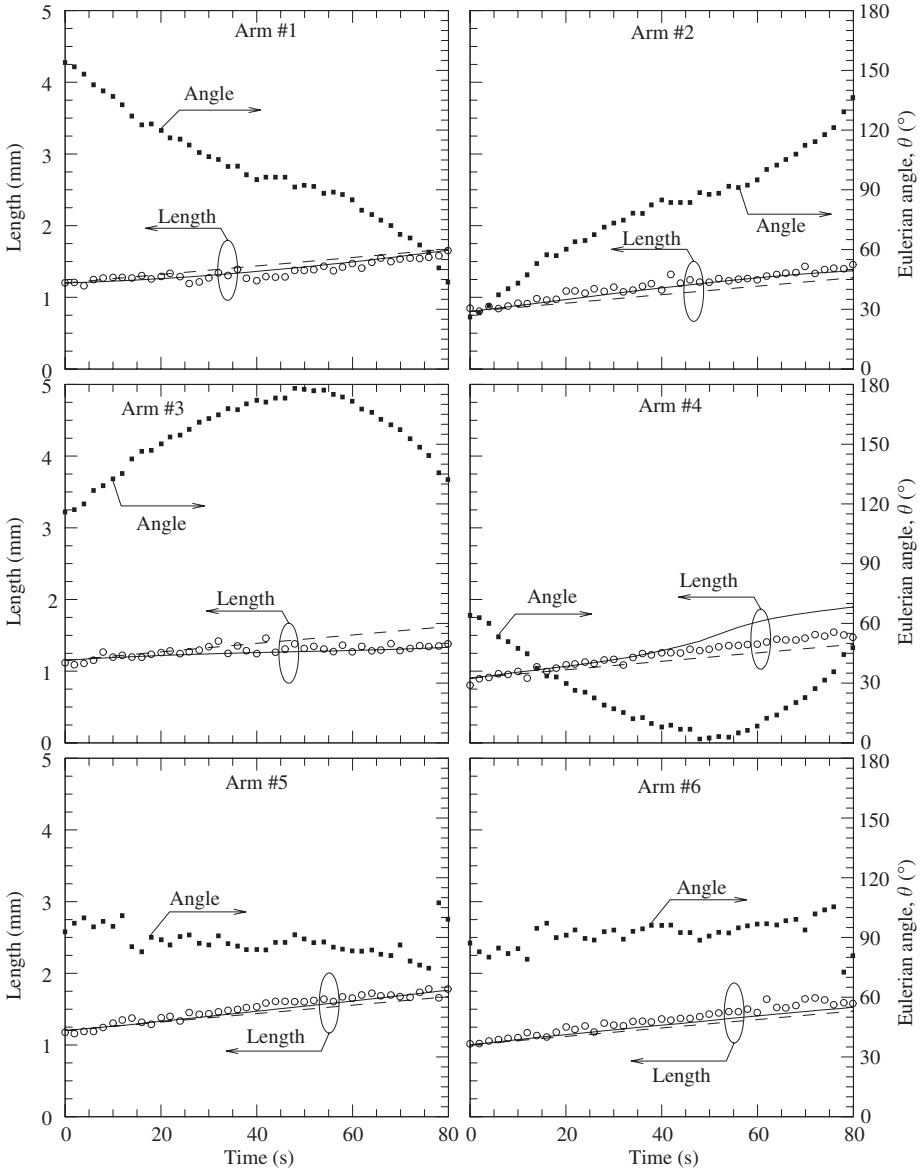

Fig. 10. Measured dendrite arm lengths (open circles) and Eulerian angles (solid squares) as a function of time for experiment 7, and predicted dendrite arm lengths from the diffusion theory (dashed line) and the convection model (solid line).

[5] and Chopra et al. [7], respectively, where the measured tip velocities were larger than the diffusion values by up to a factor of about 3.

For melt flowing directly opposite to the dendrite tip growth direction (i.e., $\theta = 0^\circ$), the two boundary layer thicknesses in Eqs. (7) and (8) are calculated from the following correlation for convection from a dendrite tip developed by Gandin et al. [18]:

$$\delta_T = \frac{2R}{aRe^b Pr^c} \quad \text{and} \quad \delta_C = \frac{2R}{a\,Re^b Sc^c}, \tag{9}$$

where the flow Reynolds number is given by $Re = 2RU/\nu$, in which ν is the kinematic viscosity of the melt, and $Pr = \nu/\alpha_l$ and $Sc = \nu/D_l = Pr\,Le$ are the Prandtl and Schmidt numbers, respectively. This correlation was obtained by fitting Eqs. (7) or (8) to the exact Stokes flow solution of Ananth and Gill [10]. The fit resulted in the following values for the constants in Eq. (9) [18]: $a = 0.5773$, $b = 0.6596$, and $c = 0.5249$.

In order to account for the dependence of the heat and solute transport from the dendrite tip on the direction of the flow relative to the dendrite arm axis, Sekerka et al. [9] and Gandin et al. [18] introduced a simple sinusoidal function into the expression for the boundary layer thickness. As noted in the previous subsection, this method would not work in predicting the dendrite tip growth velocities measured in the wake of the crystals, because it results in tip velocities that are always greater than the diffusion value. In fact, any change to the equations for the boundary layer thicknesses, Eq. (9), would have that effect, since the exponential integral function that accounts for the convection effect is always positive. A more complete

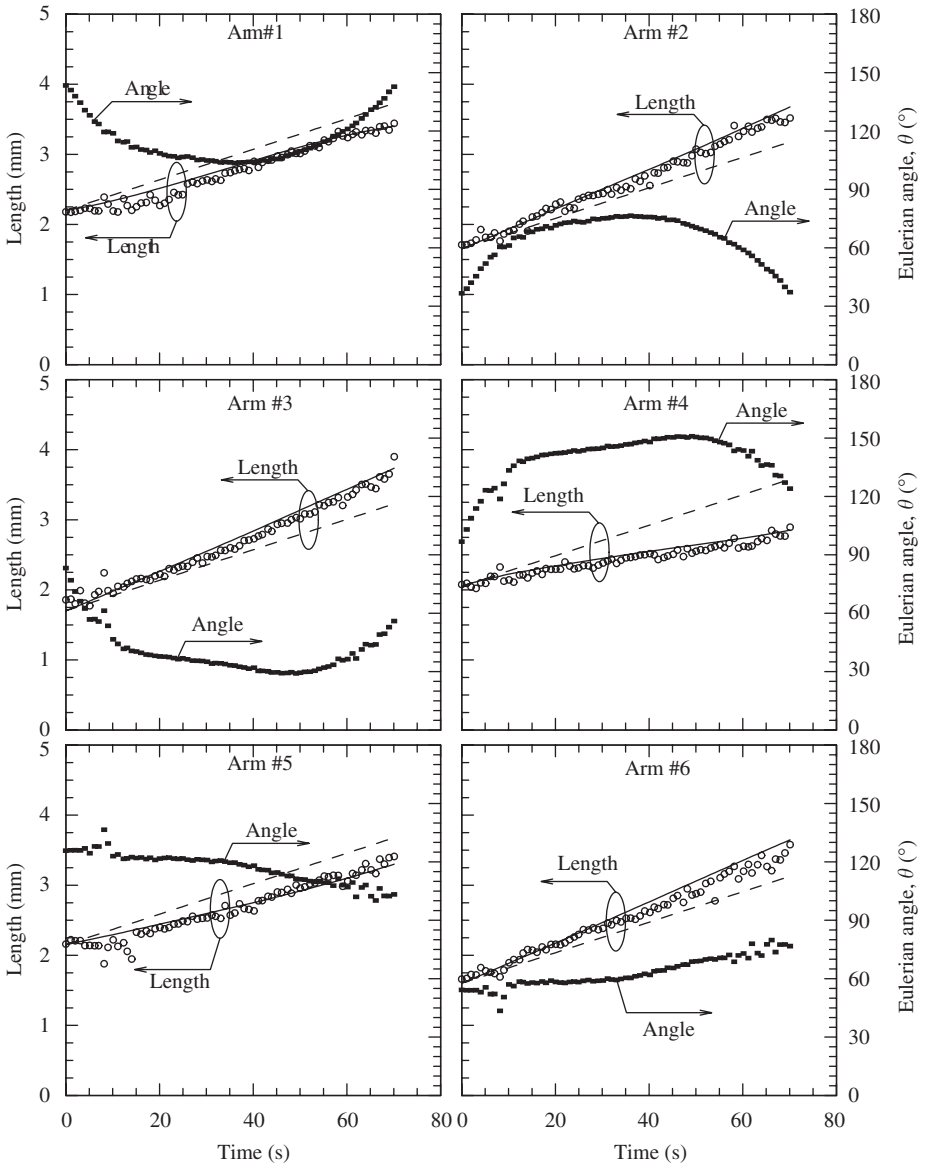

Fig. 11. Measured dendrite arm lengths (open circles) and Eulerian angles (solid squares) as a function of time for experiment 8, and predicted dendrite arm lengths from the diffusion theory (dashed line) and the convection model (solid line).

theory would not only include the flow angle effect on the boundary layer thicknesses, but would also need to account for the reduction of the melt undercooling in the wake of a crystal due to heat and solute rejection from upstream dendrite arms. In lieu of such a theory, a more practical approach is pursued here which is simply intended to provide a framework for correlating the measured tip velocities. As can be seen in Eqs. (7) and (8), a flow direction factor $f(\theta)$ is added to the term in the stagnant film solution that accounts for the effect of convection. It is added to that term only, so that in the absence of flow the angle does not play a role. The flow direction factor should have the properties that (i) $f(\theta = 0^\circ) = 1$, such that the solution for flow opposite to the dendrite tip growth direction is recovered; (ii) $f(\theta) > 0$ ($f(\theta) < 0$) for angles that correspond to measured dendrite tip velocities that are greater (smaller) than the diffusion value; and (iii) $f(\theta) = 0$ for angles where $v_{meas}/v_{diff} = 1$. By allowing $f(\theta)$ to be negative, it is possible to predict tip velocities that are less than the diffusion value, as observed in the experiments.

As a first step in determining the flow direction factor, individual values of $f(\theta)$ were calculated for each of the measured dendrite tip growth velocities listed in Table 2. This was accomplished in a trial-and-error process by choosing different values for $f(\theta)$ until the measured and predicted tip growth velocities agreed. The flow direction factors calculated in this manner are plotted in Fig. 14 (open circles). Despite the scatter, it can be seen that $f(\theta)$ generally decreases with increasing flow angle, θ. As expected, the values are generally positive for angles below about 90°, and negative for $\theta > 90^\circ$. Unfortunately, no discrete dendrite tip growth velocity data are available

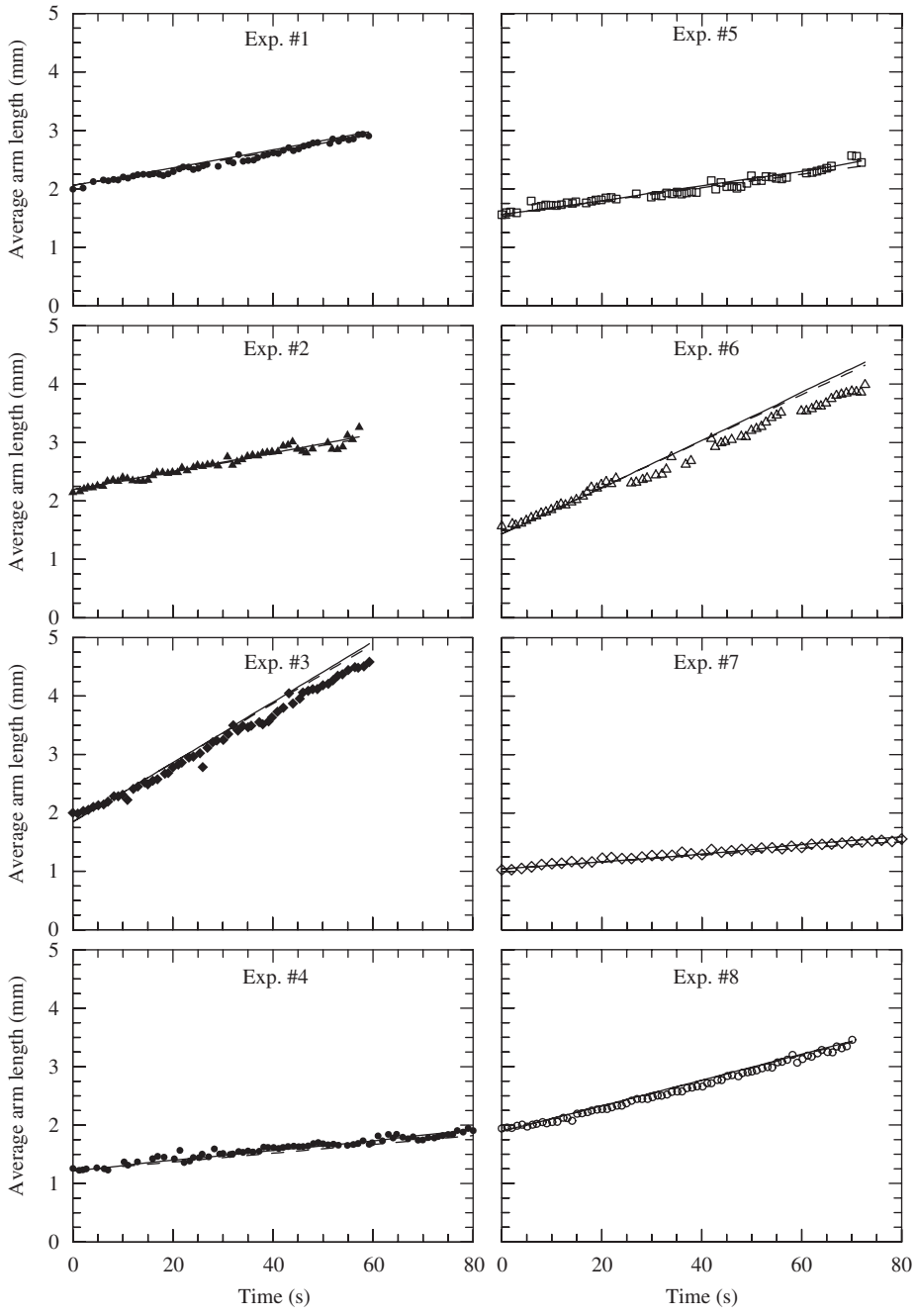

Fig. 12. Measured dendrite arm lengths averaged over all six arms (symbols), and predicted average dendrite arm lengths from the diffusion theory (dashed line) and the convection model (solid line).

for small angles, because the time periods during which an equiaxed crystal settles with a primary dendrite arm pointing downwards are always very short (see Figs. 4–11). Nonetheless, it does not seem unreasonable to assume that $f(\theta) = 0^\circ = 1$. Since all calculated $f(\theta)$ values fall below unity, it is clear that flow directly opposite to the dendrite growth direction ($\theta = 0^\circ$) indeed provides the maximum enhancement in the heat and solute transport from the dendrite tip. The scatter in the $f(\theta)$ data in Fig. 14 may be explained in part by the fact that the measured dendrite tip growth velocities represent averages over an angle interval of $\pm 15^\circ$ and a settling speed interval of ± 0.5 mm/s. Another reason for the scatter could be that the present model does not take into account the overall size of an equiaxed crystal and the rotational angle of the dendrite arms in the plane perpendicular to gravity, which can be expected to affect both the flow pattern and the magnitude of the reduction of the undercooling in the wake of a crystal. However, scatter also exists for small flow angles, for which the tip growth is likely to be unaffected by upstream dendrite arms. For such small flow angles, including the dependency of the boundary layer thickness on the flow angle as in

Table 2
Measured settling speeds, U, dendrite tip growth velocities, v_t and Eulerian angles, θ, averaged over the time periods listed; the dendrite arm numbers refer to Figs. 4–11

Experiment	Dendrite arm	Time period (s)	U (mm/s)	v_t (μm/s)	θ (°)
1	1	30–60	4.9	13.3	158
	2	0–30	4.0	16.3	33
	2	30–60	4.9	25.5	22
	3	0–30	4.0	26.6	63
	3	30–60	4.9	15.8	71
	4	0–30	4.0	9.3	118
	4	30–60	4.9	20.0	109
	5	0–30	4.0	20.1	74
	5	30–60	4.9	17.1	79
	6	0–30	4.0	14.1	106
	6	30–60	4.9	12.1	101
2	1	0–30	4.6	11.4	134
	2	0–30	4.6	20.8	46
	2	30–60	5.8	17.2	39
	3	0–30	4.6	29.6	53
	4	0–30	4.6	7.34	127
	4	30–60	5.8	19.1	123
	5	0–30	4.6	19.2	67
	5	30–60	5.8	23.2	75
	6	0–30	4.6	10.7	113
	6	30–60	5.8	11.4	105
3	1	5–25	3.9	11.0	149
	1	40–60	6.1	72.7	34
	2	5–25	3.9	55.7	31
	2	40–60	6.1	12.4	146
	3	6–16	3.8	41.7	80
	3	25–35	4.9	73.8	29
	3	45–60	6.4	32.5	119
	4	6–16	3.8	40.2	101
	4	25–40	4.9	26.3	151
	4	45–60	6.4	63.3	61
	5	0–20	3.7	57.1	64
	5	20–35	4.8	60.7	95
	5	42–60	6.3	28.4	109
	6	0–20	3.7	42.3	116
	6	20–35	4.8	39.7	86
	6	42–60	6.3	61.9	71
4	1	0–20	2.8	5.5	162
	1	50–78	3.9	13.6	19
	2	0–20	2.8	16.4	18
	2	50–78	3.9	5.2	161
	3	22–42	3.2	3.3	156
	3	42–58	3.6	3.1	123
	4	22–42	3.2	16.5	24
	4	42–60	3.6	3.7	57
	4	60–72	3.9	8.5	94
	5	0–40	3.0	8.6	98
	5	40–80	3.8	6.0	88
	6	0–40	3.0	7.7	82
	6	40–80	3.8	8.1	92
5	1	0–20	2.8	4.7	138
	1	35–55	3.5	22.8	30
	2	0–20	2.8	17.7	42
	2	35–55	3.5	4.9	150
	3	10–25	3.0	8.8	98
	3	25–50	3.4	17.2	74
	3	50–70	3.8	18.5	85
	4	10–25	3.0	13.2	82
	4	25–50	3.4	10.5	106
	5	15–33	3.1	24.4	27
	5	52–72	3.9	7.7	162
	6	10–35	3.1	1.0	153
	6	52–72	3.9	17.9	18
6	1	5–20	2.4	10.7	143
	1	38–55	3.9	44.4	33
	1	65–78	5.0	26.3	124
	2	5–20	2.4	35.5	37
	2	38–55	3.9	9.5	147
	2	65–78	5.0	59.4	56
	3	22–40	3.2	42.6	30
	3	65–78	5.0	19.3	140
	4	22–40	3.2	10.1	150
	4	65–78	5.0	36.0	40
	5	10–28	2.7	48.5	62
	5	45–65	4.2	36.0	111
	5	65–78	5.0	43.3	72
	6	12–26	2.7	19.7	119
	6	45–65	4.2	60.0	70
	6	65–78	5.0	20.1	109
7	1	32–65	2.0	6.3	92
	2	12–32	1.8	8.3	64
	2	32–65	2.0	5.0	88
	3	7–28	1.8	3.4	146
	3	32–65	2.0	0.8	173
	4	7–28	1.8	10.4	34
	4	32–65	2.0	8.4	8
	4	65–75	2.1	8.0	18
	5	0–40	1.8	9.1	91
	5	40–80	2.1	4.4	86
	6	0–40	1.8	8.5	90
	6	40–80	2.1	7.2	94
8	1	10–30	2.4	17.8	110
	1	35–60	3.3	22.2	109
	2	10–30	2.4	27.3	70
	2	35–60	3.3	31.9	71
	3	10–35	2.5	22.8	37
	3	35–60	3.3	29.8	32
	4	10–35	2.5	10.7	143
	4	35–60	3.3	8.5	149
	5	10–35	2.5	16.8	121
	5	35–60	3.3	24.7	114
	6	10–35	2.5	24.4	59
	6	35–60	3.3	29.7	66

Refs. [9,18] may have resulted in better predictions. Since the present modification of the stagnant film solution of Cantor and Vogel [26] does not explicitly account for any of these effects, it can only be viewed as a first attempt in correlating the measured tip growth velocities.

In order to obtain an analytical relation for $f(\theta)$, a fifth order polynomial given by

$$f(\theta) = 1 + \sum_{i=1}^{5} a_i \theta^i \tag{10}$$

Table 3
Properties of SCN and SCN–acetone alloys

	Symbol	Property	Value	Reference
SCN	T_m	Melting point (K)	331.233	[5]
	α_l	Liquid thermal diffusivity ($\mu m^2/s$)	1.134×10^5	[5]
	Γ	Gibbs–Thomson coefficient (K μm)	6.525×10^{-2}	[5]
	L_f/c_l	Unit supercooling (K)	23.13	[5]
	d_0	Thermal capillary length (μm)	2.821×10^{-3}	[5]
	Pr	Prandtl number	23.1	[10]
SCN–acetone	D_l	Liquid mass diffusivity ($\mu m^2/s$)	1.27×10^3	[22]
	m	Liquidus slope (K/wt%)	−2.8	[22]
	k	Equilibrium partition ratio (wt%/wt%)	0.1	[22]
	Le	Lewis number	89.3	
	Sc	Schmidt number	2062.6	
	ρ_l	Liquid density (g/cm^3): $\rho_l = 1.0334 - (7.81 \times 10^{-4} + 3.04 \times 10^{-6} C_0)T_0 - 2.114 \times 10^{-3} C_0 - 1.4 \times 10^{-5} C_0^2$ (T_0 in °C; C_0 in wt%)		[20]
	ρ_s	Solid density (g/cm^3): $\rho_s = 1.048 - 5.52 \times 10^{-4} T_0$ (T_0 in °C)		[20]

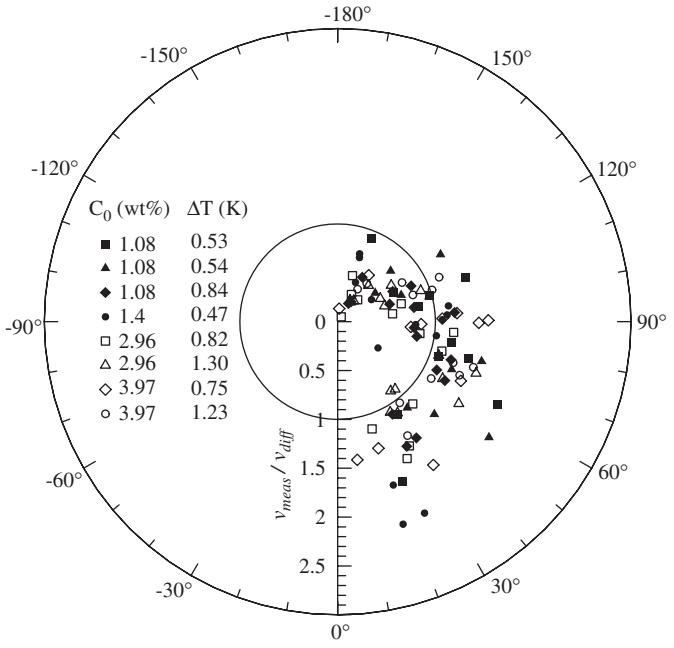

Fig. 13. Ratio of measured dendrite tip velocities (see Table 2) to tip velocities predicted from the diffusion theory as a function of the Eulerian angle for all eight experiments.

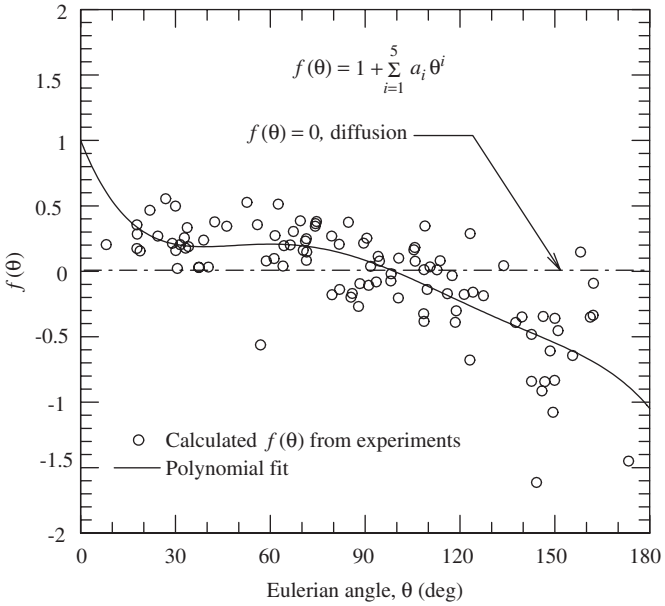

Fig. 14. Flow direction factor as a function of the Eulerian angle.

was fit to the data in Fig. 14, where θ is in degrees. The resulting coefficients are given by: $a_1 = -6.11 \times 10^{-2}$, $a_2 = 1.67 \times 10^{-3}$, $a_3 = -2.02 \times 10^{-5}$, $a_4 = 1.065 \times 10^{-7}$, and $a_5 = -2.08 \times 10^{-10}$. It can be seen in Fig. 14 that the line representing this fit varies from 1 to about −1, with the zero crossing at about 98°. Using the above relation for $f(\theta)$ in Eqs. (7) and (8), the dendrite tip growth velocities predicted by the convection model are compared to the measured values (see Table 2) in Fig. 15. It can be seen that the measured and predicted tip velocities agree to within about $\pm 10\,\mu m/s$ over the entire range of measured velocities. This good agreement is achieved despite the seemingly large scatter in the $f(\theta)$ data in Fig. 14. It indicates that the addition of the flow direction factor in Eqs. (7) and (8), together with Eqs. (9) and (10), is reasonably effective in correlating the tip growth velocities measured in the settling experiments.

A stringent test of the present convection model is obtained by comparing its predictions with the measured dendrite arm length variations shown in Figs. 4–11. For a given experiment, the instantaneous tip growth velocity was calculated from the above model as a function of the measured instantaneous settling speed, U, and flow angle, θ. Since U and θ vary continuously during an experiment, the predicted tip velocity is not constant and the dendrite arm length must be obtained by numerical integration of the equation $dL/dt = v_t$. The result is shown as continuous solid lines in Figs. 4–11. In all cases, good agreement can be observed between the measured and predicted arm length

variations. The agreement is particularly impressive for cases where the convection model predicts tip growth velocities that vary strongly during an experiment and/or are very different from the diffusion values. Examples are provided by arm #1 in Figs. 4–6, arms #2 and #4 in Figs. 6 and 9, and arm #4 in Fig. 11.

Since the individual dendrite arm lengths are predicted correctly, it is not surprising that the measured and predicted *average* arm lengths for each equiaxed crystal agree as well. This is demonstrated in Fig. 12, where the average arm lengths from the convection model are plotted as solid lines. It can be seen that differences between the convection and diffusion model results for the average arm length are negligibly small, and both agree with the measurements. This indicates that the present $f(\theta)$ function, Eq. (10), is sufficiently anti-symmetric about $\theta = 90^\circ$. Such anti-symmetry is needed so that the increases in the tip growth velocities due to convection for the three arms with a flow angle less than 90° approximately cancel the reductions for the three arms with $\theta > 90^\circ$, and the average corresponds to the diffusion limit ($f(\theta) = 0$). Overall, the above comparisons establish some confidence in the present convection model.

5. Conclusions

The present measurements of the tip growth velocities of equiaxed dendritic SCN–acetone crystals settling in an undercooled melt reveal a number of interesting effects that apparently contradict previous measurements and models. The average tip growth velocity of the six primary dendrite arms of an equiaxed crystal is found to be constant, despite significant settling speed increases and crystal rotation during an experiment. Furthermore, this average tip growth velocity is found to be in almost perfect agreement with the prediction from the standard free dendritic growth theory for purely diffusive heat and solute transport (with $\sigma^* = 0.02$), for all melt undercoolings and acetone concentrations. This agreement is remarkable because the individual dendrite arms grow at velocities that are not only very different from the diffusion value, but are also not constant during settling. This finding differs from the results of previous experiments with NH_4Cl–H_2O solutions [14–16], even though the ratio of the flow velocity to the growth velocity is in a similar range. Unlike the previous NH_4Cl–H_2O results, the present comparisons are not hampered by large uncertainties in the properties (e.g., the Gibbs–Thomson coefficient) or the dendrite tip selection parameter, σ^*.

The present experimental results are also used to develop a model for the effect of convection on dendrite tip growth that takes the flow angle effect into account. Unlike previous models [9,18], it can predict growth velocities that are smaller than the diffusion value. Such growth velocities are generally observed for dendrite tips in the wake of an equiaxed crystal. However, this model should not be interpreted as a rigorous theory, because the present measurements were used to calibrate it. Hence, it is not known whether it applies to conditions other than those of the present experiments. Nonetheless, it accurately predicts the measured dendrite tip growth velocities for all flow velocities and flow angles (with $\sigma^* = 0.02$). Moreover, by using the measured settling speed and flow angle variations as input, the model is shown to predict well the tip growth velocity variations that occur during the experiments. It is recommended that a rigorous theory of equiaxed dendritic growth with melt flow be developed.

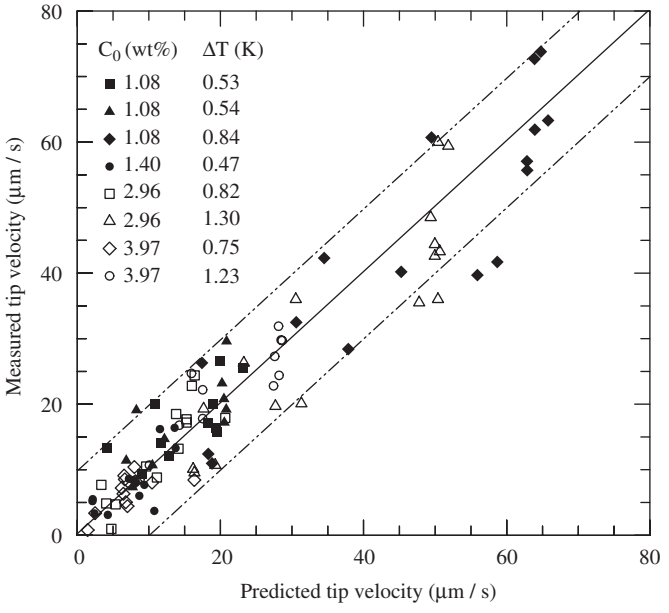

Fig. 15. Comparison of measured (see Table 2) and predicted dendrite tip velocities.

Acknowledgment

This work was supported by NASA under contracts NCC8-199 and NNM04AA18G.

References

[1] M. Rappaz, Int. Mater. Rev. 34 (1989) 93.
[2] C. Beckermann, C.Y. Wang, Ann. Rev. Heat Transfer 6 (1995) 115.
[3] C. Beckermann, Int. Mater. Rev. 47 (2002) 243.
[4] C.Y. Wang, C. Beckermann, Metall. Mater. Trans. 27A (1996) 2754.
[5] M.B. Koss, J.C. LaCombe, L.A. Tennenhouse, M.E. Glicksman, E.A. Winsa, Metall. Mater. Trans. 30A (1999) 3177.
[6] S.C. Huang, M.E. Glicksman, Acta Metall. 29 (1981) 701.
[7] M.A. Chopra, M.E. Glicksman, N.B. Singh, Metall. Trans. 19A (1988) 3087.
[8] Y.W. Lee, R. Ananth, W.N. Gill, J. Crystal Growth 132 (1993) 226.
[9] R.F. Sekerka, S.R. Coriell, G.B. McFadden, J. Crystal Growth 154 (1995) 370.
[10] R. Ananth, W.N. Gill, J. Crystal Growth 108 (1991) 173.
[11] Q. Li, C. Beckermann, J. Crystal Growth 236 (2002) 482.
[12] Y.W. Lee, R.N. Smith, M. Glicksman, M.B. Koss, Ann. Rev. Heat Transfer 7 (1996) 59.
[13] R. Ananth, W.N. Gill, J. Crystal Growth 179 (1997) 263.
[14] A. Ramani, C. Beckermann, Scripta Metall. 36 (1997) 633.

[15] B. Appolaire, V. Albert, H. Combeau, G. Lesoult, Acta Mater. 46 (1998) 5851.
[16] B. Appolaire, V. Albert, H. Combeau, G. Lesoult, ISIJ Int. 39 (1999) 263.
[17] J.M. Liu, Z.G. Liu, G.C. Wu, Scripta Metall. 32 (1995) 445.
[18] Ch.A. Gandin, G. Guillemont, B. Appolaire, N.T. Niane, Mater. Sci. Eng. A 342 (2003) 44.
[19] X. Tong, C. Beckermann, A. Karma, Q. Li, Phys. Rev. E 63 (2001) 061601.
[20] D.L. Ceynar, C. Beckermann, J. Crystal Growth 222 (2001) 380.
[21] J. Lipton, M.E. Glicksman, W. Kurz, Mater. Sci. Eng. 65 (1984) 57.
[22] J. Lipton, M.E. Glicksman, W. Kurz, Metall. Trans. A 18A (1987) 341.
[23] J. Lipton, W. Kurz, R. Trivedi, Acta Metall. 35 (1987) 957.
[24] R. Trivedi, W. Kurz, Int. Mater. Rev. 39 (1994) 49.
[25] D.S. Schrage, J. Crystal Growth 205 (1999) 410.
[26] B. Cantor, A. Vogel, J. Crystal Growth 41 (1977) 109.